Journal of Solid State Chemistry 183 (2010) 128–135

Contents lists available at ScienceDirect

Journal of Solid State Chemistry

journal homepage: www.elsevier.com/locate/jssc

Crystallization of niobium germanosilicate glasses

Rodrigo Santos [a], Luís F. Santos [a,*], Rui M. Almeida [a], Joachim Deubener [b], Lothar Wondraczek [c]

[a] Departamento de Engenharia de Materiais/ICEMS, Instituto Superior Técnico/TU Lisbon, Av. Rovisco Pais, 1, 1049-001 Lisbon, Portugal
[b] Institute of Non-Metallic Materials, Clausthal University of Technology, Clausthal-Zellerfeld, Germany
[c] Department of Materials Science, Glass and Ceramics, University of Erlangen-Nuremberg, 91058 Erlangen, Germany

ARTICLE INFO

Article history:
Received 18 July 2009
Received in revised form
24 October 2009
Accepted 29 October 2009
Available online 10 November 2009

PACS:
42.70.Ce
81.05.Pj
61.46.Hk

Keywords:
Germanosilicate glasses
Transparent glass ceramics
Nanocrystallization

ABSTRACT

Niobium germanosilicate glasses are potential candidates for the fabrication of transparent glass ceramics with interesting non-linear optical properties. A series of glasses in the $(Ge,Si)O_2$–Nb_2O_5–K_2O system were prepared by melting and casting and their characteristic temperatures were determined by differential thermal analysis. Progressive replacement of GeO_2 by SiO_2 improved the thermal stability of the glasses. Depending on the composition and the crystallization heat-treatment, different nanocrystalline phases—$KNbSi_2O_7$, $K_3Nb_3Si_2O_{13}$ and $K_{3.8}Nb_5Ge_3O_{20.4}$ could be obtained. The identification and characterization of these phases were performed by X-ray diffraction and Raman spectroscopy.

The 40 GeO_2–10 SiO_2–25 Nb_2O_5–25 K_2O (mol%) composition presented the higher ability for volume crystallization and its nucleation temperature was determined by the Marotta's method. An activation energy for crystal growth of ~529 kJ/mol and a nucleation rate of $9.7 \times 10^{18}\,m^{-3}\,s^{-1}$ was obtained, for this composition. Transparent glass ceramics with a crystalline volume fraction of ~57% were obtained after a 2 h heat-treatment at the nucleation temperature, with crystallite sizes of ~20 nm as determined by transmission electron microscopy.

1. Introduction

Glass ceramics can be defined as a group of polycrystalline ceramic materials which, depending on the glass matrix and the crystalline phases present, can achieve optimized mechanical, thermal, electrical or optical properties [1]. Such materials are usually obtained through the controlled crystallization of glass, which remains as a minority phase in the ceramic. The development of new glass ceramics containing crystalline phases with non-linear optical properties has increased in the last decades due to their potential application in photonics, such as tunable waveguides or optical switching in all-optical and electro-optical systems [2–5]. Photonics may be defined as the technology of information processing and transfer by means of light and non-linear optical materials are the basis of this technology [1], so it is of great interest to study such glass ceramic materials. High optical transparency is also very important to observe electro-optic phenomena [6], thus, in the fabrication of transparent glass ceramics, a good glass-forming matrix is required and controlled crystallization is necessary [4] to avoid loss of transparency. Niobium silicate and niobium germanate glass systems have been studied by several authors [3–14] and transparent glass ceramics presenting second harmonic generation (SHG) effect have been obtained [7,10]. One of the peculiarities of these systems is their large glass-forming region which, in the case of the $SiO_2 \cdot Nb_2O_5 \cdot K_2O$ system, extends to as little as 20 mol% silica, taking advantage of the fact that niobium oxide may play the role of both glass network modifier and network former. Actually, the coordination number of niobium increases from 4 to 6 as the concentration of niobium oxide increases in silicate and germanosilicate glasses, forming a three-dimensional structure of NbO_6 octahedra connected to SiO_4 and/or GeO_4 tetrahedra [6,15]. While the $SiO_2 \cdot Nb_2O_5 \cdot K_2O$ and the GeO_2–Nb_2O_5–K_2O systems have been extensively studied, there is only one reference regarding the mixed GeO_2–SiO_2–Nb_2O_5–K_2O system [11] to the best of author's knowledge. Since these systems are among the few oxide systems in which nucleation occurs to an extent that enables transparency while attaining a high crystallite fraction, it is important to study such systems and their crystallization behavior. Table 1 presents the niobium silicate and niobium germanate glass-ceramic systems found in the literature with their respective characteristic temperatures (glass transition, T_g, crystallization onset, T_x, and crystallization peak, T_p), plus the crystalline phases present and respective SHG intensity. It can be seen that the highest values of SHG have been obtained in the system $SiO_2 \cdot Nb_2O_5 \cdot K_2O$ for non-transparent crystallized samples.

Thus, the purpose of this work is to study the substitution of GeO_2 for SiO_2 within the mixed GeO_2–SiO_2–Nb_2O_5–K_2O system, for the preparation of glasses and glass ceramics.

* Corresponding author. Fax: +351 218418132.
E-mail address: luis.santos@ist.utl.pt (L.F. Santos).

0022-4596/$ - see front matter © 2009 Elsevier Inc. All rights reserved.
doi:10.1016/j.jssc.2009.10.031

Table 1
Niobium silicate and niobium germanate glass systems and respective characteristic temperatures, SHG intensity and crystalline phases.

System	Composition	Ref.	T_g	T_x	T_p	SHG[d]	Crystalline phases
Si.Nb.Li	46.1Si–15.4Nb–38.5Li	[14]	522				$LiNbO_3$
	43.1Si–17.7Nb–39.2Li		528				
	40Si–20Nb–40Li		532				
	45Si–25Nb–30Li		537				
Si.Nb.K	52Si–24Nb–24K	[9]	688				$K_3Nb_3Si_2O_{13}$, $KNbSi_2O_7$
	50Si–27Nb–23K		684				
	50Si–23Nb–27K		674				
Si.Nb.K	20Si–40Nb–40K	[4]	567		626	235[b]	$KNbO_3$, $K_3Nb_3Si_2O_{13}$, $KNbSi_2O_7$
	25Si–37.5Nb–37.5K		587		672	58[b]	
	33.4Si–33.3Nb–33.3K		611		708		
	40Si–30Nb–30K		634		730	0.5[b]	
	50Si–25Nb–25K		672		784	1.7[b]	
	60Si–20Nb–20K		704		861	69[b]	
	66.7Si–16.6Nb–16.6K		707			300[b]	
	40Si–20Nb–40K		545			54[b]	
	35Si–25Nb–40K		551		693	20[b]	
	30Si–25Nb–45K		512		589		
Si.Nb.K	66.6Si–16.7Nb–16.7K	[7,8]	733			0.08[a]	$KNbSi_2O_7$
	63.6Si–18.2Nb–18.2K		724			0.6[a]	
	60Si–20Nb–20K		721			0.8[a]	
	55.6Si–22.2Nb–22.2K		705			0.9[a]	
	50Si–25Nb–25K		688			1.2[a]	
Si.Nb.K	40Si–30Nb–30K	[12]	657				$K_3Nb_3Si_2O_{13}$
Ge.Nb.Li	45Ge–30N–25Li	[2]	550				$LiNbO_3$, Li_8GeO_6
	45Ge–30Nb–25Li+10Al		560				
	40Ge–30Nb–30Li+10Al		540				
	45Ge–25Nb–30Li		530				
Ge.Nb.K.Na	50Ge–25Nb–25K	[13]	622	668		0[b]	$Na_xK_{1-x}NbO_3$, $NaNbO_3$, $NaNbGeO_5$, $K_{3.8}Nb_5Ge_3O_{20.4}$
	50Ge–25Nb–20K–5Na		607	678		0[b]	
	50Ge–25Nb–15K–10Na		600	702		0[b]	
	50Ge–25Nb–10K–15Na		587	751		6[b]	
	50Ge–25Nb–5K–20Na		589	765		1.5[b]	
	50Ge–25Nb–25Na		588	781		0[b]	
Ge.Nb.K	60Ge–20Nb–20K	[3,10]	625	732			$K_{3.8}Nb_5Ge_3O_{20.4}$
	50Ge–20Nb–30K		592	692			
	50Ge–25Nb–25K		622	668		~0.01[c]	
	50Ge–30Nb–20K		627	697			
	40Ge–30Nb–30K		612	653			
Si.Ge.Nb.K	50Ge–25Nb–25K	[11]	619		679		$K_{3.8}Nb_5Ge_3O_{20.4}$, $K_{3.8}Nb_5(Ge,Si)_3O_{20.4}$
	25Si–25Ge–25Nb–25K		655		720		
	50Si–25Nb–25K		670		761		

Note: Li–Li_2O, Nb–Nb_2O_5, Si–SiO_2, K–K_2O, Ge–GeO_2, Na–Na_2O, Al–Al_2O_3.

[a] SHG values measured in transparent crystallized samples.
[b] SHG values measured in non-transparent crystallized samples.
[c] SHG values measured in transparent crystallized samples induced by an outside alternating electric field.
[d] SHG intensity, $I_{2\omega}/I_{2\omega}$ (α-quartz).

2. Experimental

Samples with the compositions shown in Fig. 1 were prepared by melting a homogeneous mixture of reagent grade K_2CO_3, Nb_2O_5, GeO_2 and SiO_2. All compositions reported in this work are nominal (starting) compositions. Melting was performed in Pt crucibles at temperatures between 1200 and 1450 °C, depending on the composition, for 50 min. Two pre-heating steps were used: the first at 400 °C for 30 min, to remove the water present in the mixture and the second at 800 °C for 40 min, in order to fully decompose the carbonates and to remove CO_2. The melts were poured onto a pre-heated graphite mould. The characteristic temperatures were determined by differential thermal analysis (DTA), with a heating rate of 10 K/min. DTA measurements were performed with Labsys from Setaram, using ~125–165 mg of glass sample in an alumina crucible, under atmospheric air, in the range 30–1050 °C. The DTA-derived characteristic temperatures are affected by an error of ± 5 °C. Crystallization was achieved by heat-treatment of the glass samples and the crystalline phases obtained were analyzed by X-ray diffraction (XRD) and Raman spectroscopy. XRD was performed with a Philips X'PERT APD, at room temperature using Cu Kα radiation generated at 40 kV and 30 mA, with a step of 1.5°/min. Raman spectra were collected in a 90° scattering geometry at room temperature, at 4 cm^{-1} resolution, with a one second integration time. The Raman system consisted of a double monochromator (Spex 1403), an argon ion laser (Spectra-Physics, mod. 2016) operating at 514.5 nm and a photomultiplier detector (Hamamatsu R928); the wavenumber accuracy is estimated at ± 2 cm^{-1}.

The crystallization mechanism of the glass samples was studied using DTA, according to the method suggested by Ray et al. [16–18]. This method studies the effects of surface and bulk crystallization, considering two different sample sizes. In fact, studies in glasses have shown that surface crystallization is predominant for particle sizes below ~50 μm, while bulk crystallization occurs when the particle size exceeds ~150 μm

[16]. Therefore, the glass samples were ground and classified into two particles sizes: small particles (S), typically less than 100 μm and large particles (L), with 0.5–2 mm. A transmission electron microscope, Hitachi H-8100 operating at 200 kV, was used for crystal size determination.

3. Results and discussion

Three series of samples were prepared, where the molar ratios of the network former to the network modifier were 50–50 (series 1), 60–40 (series 2) and 40–60 (series 3), while all compositions maintained an Nb_2O_5:K_2O ratio of 1:1 (Fig. 1). All samples were easily vitrifiable in bulk form under the experimental conditions used, exhibiting good transparency as observed in Fig. 2 for the series 1 samples.

3.1. Heat treatments

Fig. 3 presents the DTA results of the series 3 compositions, whose characteristic temperatures are given in Table 2. The values of T_g and T_x, as well as the thermal stability parameter ($T_x - T_g$), increased with the silica content. Glass samples were heat treated, at temperatures between the first and the second crystallization peaks (between ~670 and ~900 °C, depending on the composition), in order to obtain only the first crystalline phase. Glass samples were heated at ~200 °C/min up to the heat-treatment temperature, where it stayed for 2 h. Cooling was done in the furnace, down to room temperature. The expected crystalline phases ($K_{3.8}Nb_5Ge_3O_{20.4}$, $KNbSi_2O_7$, $K_3Nb_3Si_2O_{13}$ and $KNbO_3$, see Table 1) were also separately prepared and their XRD patterns and Raman spectra were obtained in order to use them as references.

3.2. X-ray diffraction

Figs. 4 and 5 present the XRD patterns for the heat treated samples of the 50 mol% former compositions and the related crystalline phases. Crystallization of the $K_{3.8}Nb_5Ge_3O_{20.4}$ phase was observed for the samples with higher germania content, while for the samples with higher SiO_2 content the predominant crystalline phase obtained was $K_3Nb_3Si_2O_{13}$. Sample 1.3 presented both crystalline phases, while sample 1.6 seems to present $KNbSi_2O_7$. In fact, this sample had the strongest peak at ~22°, which might be assigned to the presence of the $KNbSi_2O_7$ crystalline phase, which shows strong diffracted intensity for this peak [4]. Series 2 compositions also present the $K_{3.8}Nb_5Ge_3O_{20.4}$ and the $K_3Nb_3Si_2O_{13}$ crystalline phases for the high germania and high silica compositions, respectively, while series 3 present a mixed phase $K_{3.8}Nb_5(Ge,Si)_3O_{20.4}$ for all compositions.

3.3. Raman spectroscopy

Fig. 6 presents the Raman spectra for the same samples of Figs. 4 and 5 plus the respective crystalline phases. It is shown that, for samples 1.1 and 1.2, only the $K_{3.8}Nb_5Ge_3O_{20.4}$ phase crystallizes, while sample 1.3 appears to yield the crystallization of both $K_{3.8}Nb_5Ge_3O_{20.4}$ and $K_3Nb_3Si_2O_{13}$, in agreement with the XRD results. The predominant crystalline phase in the heat treated high silica samples of series 1 is $K_3Nb_3Si_2O_{13}$, but, contrary to the information obtained by XRD, sample 1.6 does not show any characteristic peak that might be related to the

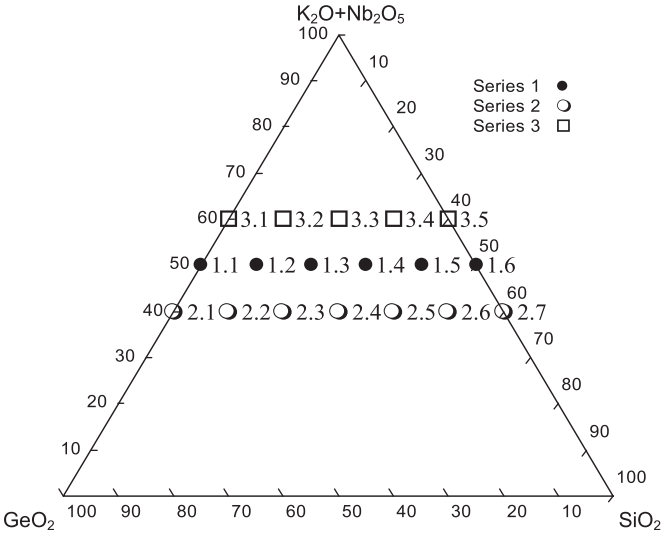

Fig. 1. Germanosilicate glass compositions prepared.

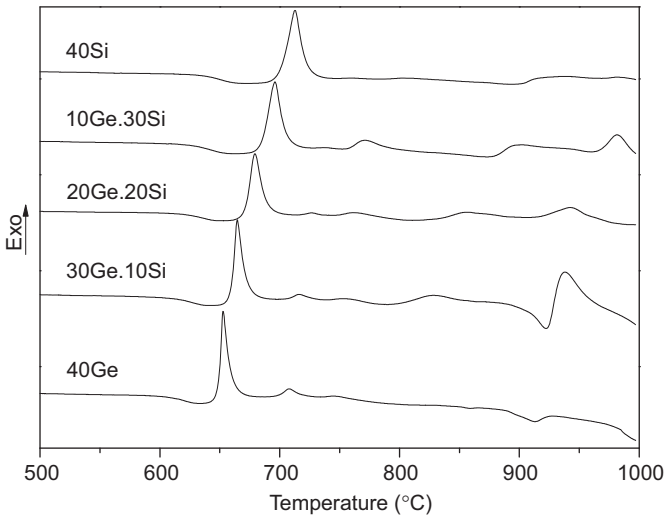

Fig. 3. DTA curves for the 40 ($GeO_2 \cdot SiO_2$)–30Nb_2O_5–30K_2O (mol%) glasses.

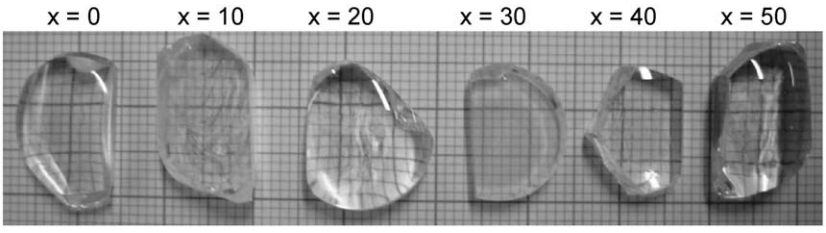

Fig. 2. (50 − x) GeO_2–x SiO_2–25Nb_2O_5–25K_2O (mol%) glasses.

Table 2
Glass compositions (in mol%) and respective characteristic temperatures: glass transition, T_g, crystallization onset, T_x, first (T_{p1}) and second (T_{p2}) crystallization peak temperatures and thermal stability parameter (T_x–T_g).

Sample	Composition (mol%)				T_g (°C)	T_x (°C)	T_{p1} (°C)	T_{p2} (°C)	T_x–T_g (°C)
	GeO_2	SiO_2	Nb_2O_5	K_2O					
1.1	50	0	25	25	624	662	675		38
1.2	40	10	25	25	638	681	693		43
1.3	30	20	25	25	645	699	715	953	54
1.4	20	30	25	25	654	713	730	914	59
1.5	10	40	25	25	659	731	749	920	72
1.6	0	50	25	25	671	749	766	952	78
2.1	60	0	20	20	626	717	735		91
2.2	50	10	20	20	646	748	785		102
2.3	40	20	20	20	654	783	814		129
2.4	30	30	20	20	667	807	849		140
2.5	20	40	20	20	678	847	–		169
2.6	10	50	20	20	693	868	–		175
2.7	0	60	20	20	700	854	902		154
3.1	40	0	30	30	611	644	653	708	33
3.2	30	10	30	30	613	650	665	716	37
3.3	20	20	30	30	622	664	679	727	42
3.4	10	30	30	30	634	680	696	737	46
3.5	0	40	30	30	640	693	713	759	53

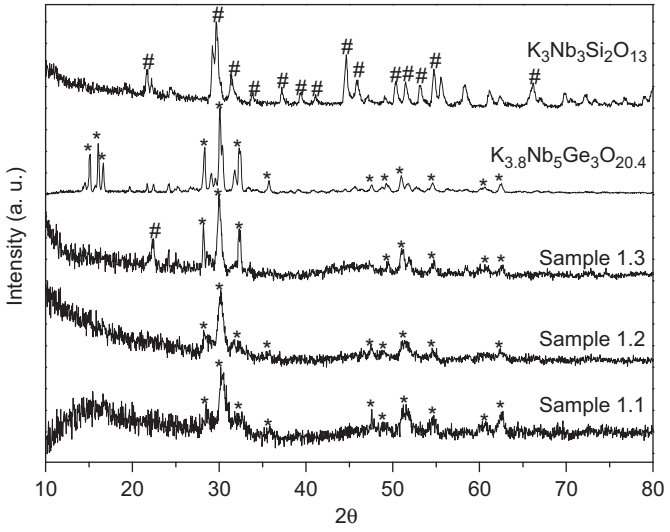

Fig. 4. XRD patterns of heat treated 1.1, 1.2 and 1.3 samples and related crystalline phases.

$KNbSi_2O_7$ crystalline phase, although there is a peak at $\sim 880\,cm^{-1}$ that cannot be assigned to any of the crystalline phases prepared. Therefore, according to the XRD and Raman data, the first crystallization peak of the DTA plot in the $(50-x)$ $GeO_2 \cdot xSiO_2 \cdot 25Nb_2O_5 \cdot 25K_2O$ system is related to the crystalline phases $K_{3.8}Nb_5Ge_3O_{20.4}$ and $K_3Nb_3Si_2O_{13}$, for the high germania and high silica content, respectively. The same result was obtained for the series 2 compositions $[(60-x)\ GeO_2 \cdot xSiO_2 \cdot 20Nb_2O_5 \cdot 20K_2O]$, although the high silica content composition is close to the stoichiometric composition of the $KNbSi_2O_7$ crystalline phase ($66.7SiO_2 \cdot 16.6Nb_2O_5 \cdot 16.6K_2O$). In fact, this composition was prepared and although a bulk glass was obtained, still the first crystalline phase to occur is $K_3Nb_3Si_2O_{13}$.

In series 3 compositions, the $K_{3.8}Nb_5Ge_3O_{20.4}$ crystalline phase is the first crystalline phase to occur, even for high silica content compositions, which suggests a mixed $K_{3.8}Nb_5(Ge,Si)_3O_{20.4}$ crystal phase for all compositions as reported by Enomoto et al. [11].

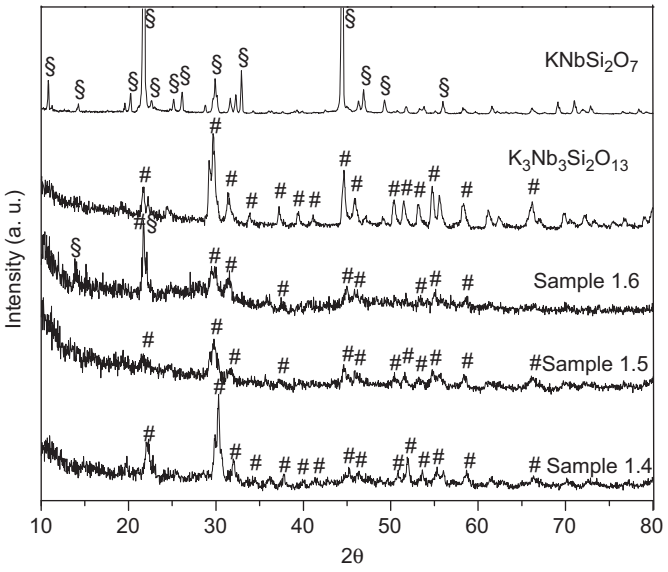

Fig. 5. XRD patterns of heat treated 1.4, 1.5 and 1.6 samples and related crystalline phases.

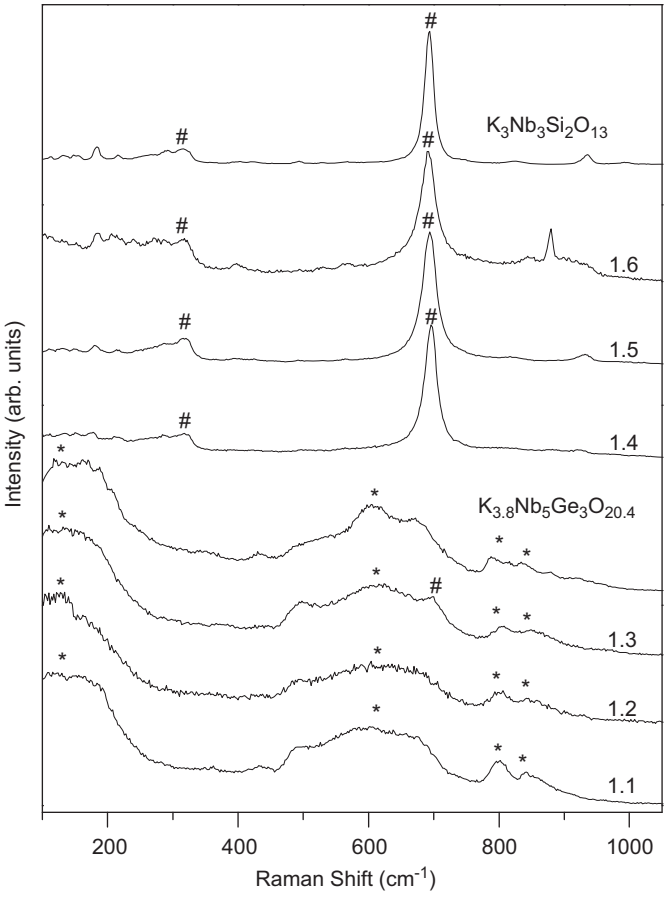

Fig. 6. Raman spectra of heat treated samples and related crystalline phases.

Therefore, transparent glass ceramics obtained through direct glass crystallization in this system can only present $K_{3.8}Nb_5Ge_3O_{20.4}$ or $K_3Nb_3Si_2O_{13}$, as first crystalline phases.

Fig. 7 presents the Raman spectra for the glassy and heat treated 1.2 composition, revealing the progressive destruction of the glass network (bands at 486, 743 and 856 cm^{-1}, related to the GeO_4 tetrahedra and NbO_6 octahedra of the glass skeleton [15],

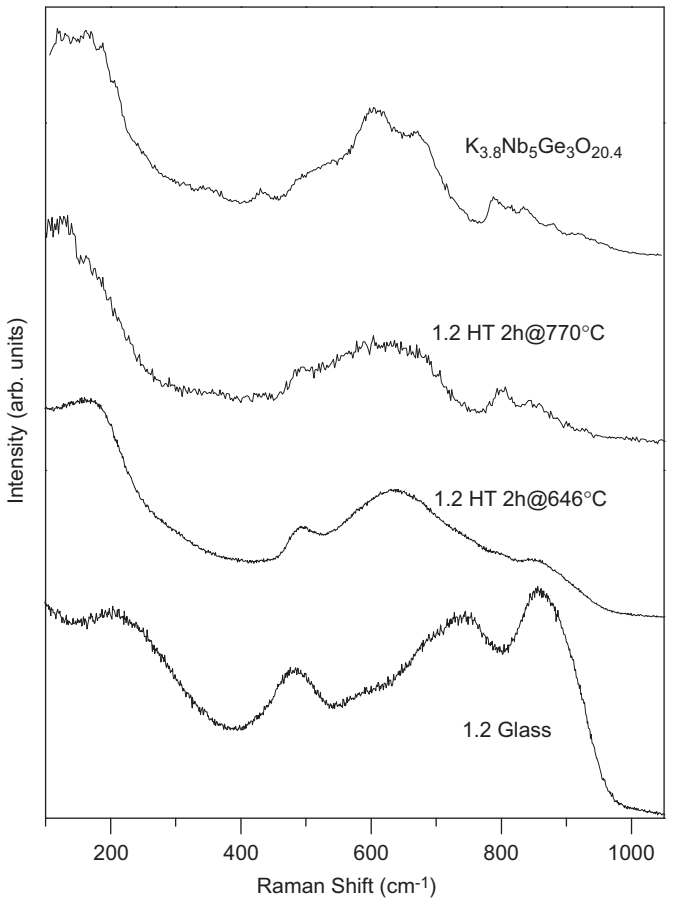

Fig. 7. Raman spectra of the 1.2 sample upon heat-treatment.

decrease their intensity with heat-treatment). On the other hand, characteristic bands of the crystalline $K_{3.8}Nb_5Ge_3O_{20.4}$ phase at ~604 and 665 cm^{-1} become predominant upon heat-treatment, being already present in the transparent glass ceramic. The high frequency bands near 800 and 836 cm^{-1} occurs only for the more prolonged heat-treatment, corresponding to a higher crystalline volume fraction.

3.4. Crystallization study

The main crystallization mechanism for the glass samples was determined using the method proposed by Ray et al. [16–18], based on the analysis of the $T_p^2/(\Delta T)_p$ parameter, where T_p is the temperature at the crystallization peak maximum and $(\Delta T)_p$ is the peak width at half maximum. According to this method, bulk crystallization is favored when $T_p^2/(\Delta T)_p$ increases with increasing particle size. DTA measurements were performed using two different particle sizes (S—< 100 μm and L—0.5–2 mm); the results obtained were normalized to the sample mass and are given in Table 3 for the series 1 compositions. The similar crystallization peaks observed for the powdered and bulk samples, indicate that there are no major changes between the DTA results of the bulk and powdered samples, revealing no dependency of the surface and, therefore, pointing to the occurrence of bulk crystallization. The $T_p^2/(\Delta T)_p$ parameter also indicated the occurrence of bulk crystallization, since it increased with particle size for all samples, with the exception of sample 1.3.

Other parameters usually used to determine the crystallization mechanism [17–20] are the Avrami parameter (n) and the crystal growth dimensionality (m), where m is defined as $n-1$ and n can be determined using the Ozawa's equation [16]:

$$\ln \varphi = -\frac{mE_c}{nRT} - \left(\frac{1}{n}\right)\ln[-\ln(1-x)] = const. \quad (1)$$

which in its modified form, for a fixed temperature T, is given by [16]:

$$\left.\frac{\partial \ln(-\ln(1-x))}{\partial \ln(\varphi)}\right|_T = -n \quad (2)$$

where x is the crystallized fraction at an arbitrary fixed temperature T, φ is the heating rate used in the DTA measurement, E_c is the activation energy for crystallization and R is the gas constant. In this case, four different heating rates were used: 5, 10, 15 and 20 °C/min. The value of x was obtained by the ratio of the partial crystallization peak area (at 693 °C—crystallization peak

Table 3
Values of the T_p, δT_p and $T_p^2/(\Delta T)_p$ parameters, obtained by the DTA analysis.

Sample		T_p (°C)	$(\Delta T)_p$ (°C)	$T_p^2/(\Delta T)_p$
1.1	S	675	8	56953
	L	676	8	57122
1.2	S	694	12	40136
	L	693	11	43659
1.3	S	715	23	22227
	L	712	24	21123
1.4	S	730	27	19737
	L	728	23	23043
1.5	S	749	25	22440
	L	747	23	24261
1.6	S	766	24	24448
	L	765	23	25445

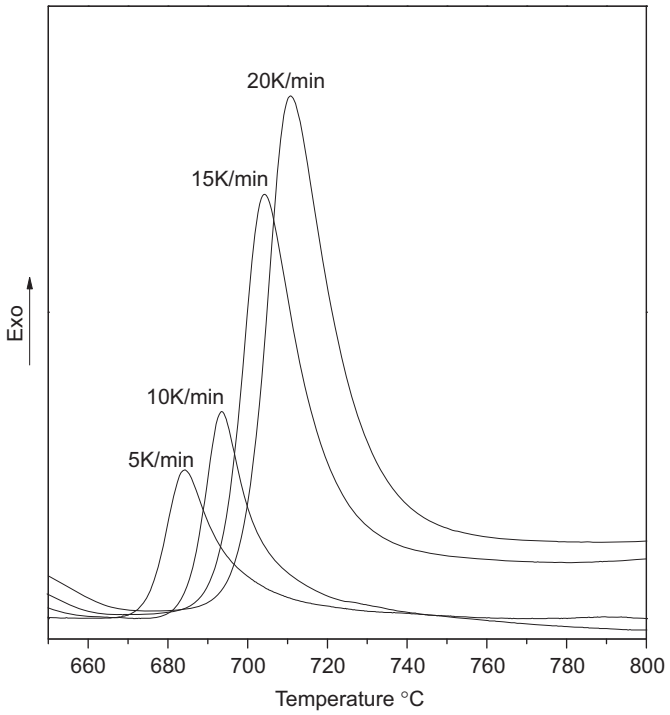

Fig. 8. DTA curves for sample 1.2 at different heating rates (φ=5, 10, 15 and 20 °C/min).

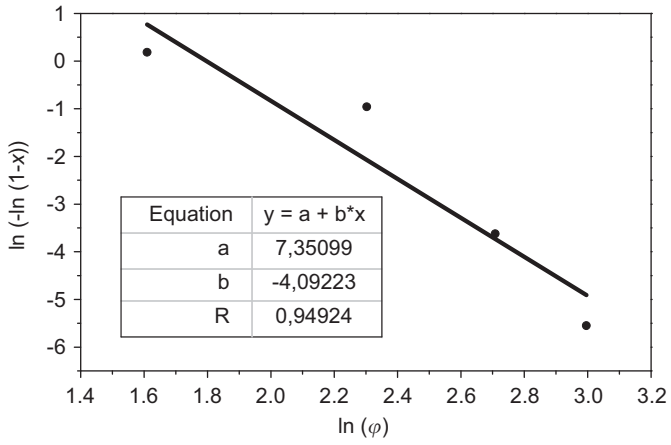

Fig. 9. Plot $\ln(-\ln(1-x))$ vs. $\ln(\varphi)$ used for the determination of n for sample 1.2.

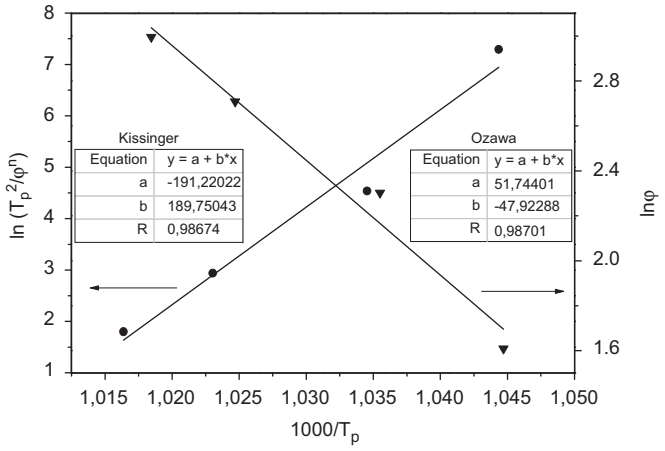

Fig. 10. Plots $\ln(T_p^2/\varphi^n)$ vs. $1/T$ and $\ln\varphi$ vs. $1/T$ used for the determination of the activation energy for crystallization of sample 1.2.

Table 4
Data obtained by the Kissinger and Ozawa modified methods to determine the activation energy for crystallization of the $40GeO_2 \cdot 10SiO_2 \cdot 25Nb_2O_5 \cdot 25K_2O$ composition.

φ (K/min)	$\ln(\varphi)$	T_p (°C)	T_p (K)	$1000/T_p$	$\ln(T_p^2/\varphi^n)$[a]
5	1.60944	684	957	1.04493	7.28986
10	2.30259	694	967	1.03413	4.53806
15	2.70805	704	977	1.02354	2.93677
20	2.99573	711	984	1.01626	1.80032

[a] Using n=4.

for the 10 °C/min heating rate, see Fig. 8), to the total area of the crystallization peak [16].

The $\ln(-\ln(1-x))$ vs. $\ln(\varphi)$ plot obtained for sample 1.2 is presented in Fig. 9, where the slope is ≈ 4, which corresponds to a value of m equal to 3. This result indicates [19] that sample 1.2 exhibited bulk nucleation at a constant rate, where the number of nuclei is inversely proportional to the heating rate. Therefore, the composition $40GeO_2 \cdot 10SiO_2 \cdot 25Nb_2O_5 \cdot 25K_2O$ was chosen for glass ceramic preparation, for which volume crystallization could be induced using suitable heat treatments.

3.5. Activation energy for crystallization

The activation energy for crystallization of sample 1.2 was calculated using the Kissinger modified equation [20]:

$$\ln\left(\frac{T_p^2}{\varphi^n}\right) = \frac{mE_c}{RT_p} + const. \quad (3)$$

and the modified form of the Ozawa's equation [19]:

$$\ln\varphi = -\frac{mE_c}{nRT_p} + const. \quad (4)$$

Fig. 8 presents the first crystallization peak obtained at different heating rates for sample 1.2, whose peak temperatures (T_p) are used to determine the activation energy for crystal growth according to Eqs. (3) and (4), with n=4 and m=3 as determined above. Table 4 presents the results according to the modified Kissinger and Ozawa methods, from where the $\ln(T_p^2/\varphi^n)$ vs. $1/T_p$ and $\ln\varphi$ vs. $1/T_p$ plots, respectively, are obtained as shown in Fig. 10. E_c is determined from the (mE_c/R) and $(-mE_c/nR)$ slopes, respectively. Using the values of m=3 and n=4, the activation energy for crystallization for sample 1.2 was determined and values of 525.9 kJ/mol for the Kissinger method and 531.3 kJ/mol for the Ozawa method were obtained. These values are in agreement with the values reported in the literature for germanate glasses: Laudisio and Catauro [21] reported an E_c value of 558 kJ/mol in the $K_2O \cdot 4GeO_2$ system, for the $K_4Ge_9O_{20}$, crystalline phase, which is similar to the $K_{3.8}Nb_5Ge_3O_{20.4}$ crystalline phase obtained for the $40GeO_2 \cdot 10SiO_2 \cdot 25K_2O \cdot 25Nb_2O_5$ composition.

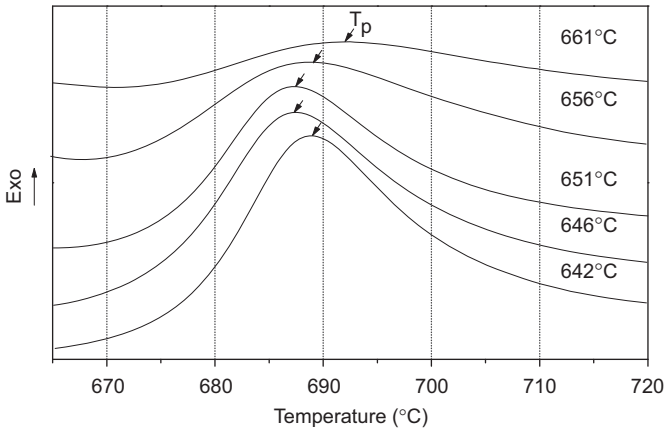

Fig. 11. First crystallization peak obtained for the different nucleation temperatures.

3.6. Temperature of maximum nucleation rate

The temperature of maximum nucleation rate was determined using the Marotta's method, which determines the relative nucleation rates by a thermal program for the glass heat-treatment, where an intermediate thermal hold is used to induce exothermic peak temperature shifts [22]. The thermal program consists of a first heating step at a constant heating rate (e.g. 10°/min), followed by a nucleation heat-treatment at a constant temperature. After this thermal hold, the samples are further heated at the same heating rate as before, above the first crystallization peak temperature. The nucleation period used was 15 min for all samples and the DTA result is presented in Fig. 11.

Data analysis focuses on shifts of the exothermic crystallization peak temperatures via Eq. (5) [23]:

$$\ln(I_0) = \frac{E_c}{R}\left(\frac{1}{T_{p1}} - \frac{1}{T_{p1}^0}\right) + const. \quad (5)$$

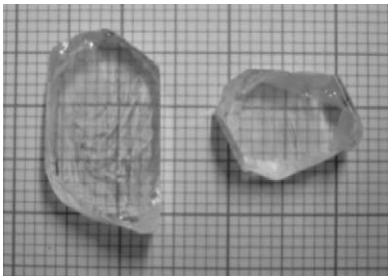

Fig. 12. On the left, the original glass sample 1.2; on the right, the glass ceramic produced with the same composition.

where I_0 is the steady-state nucleation rate, T_{p1} and T_{p1}^0 are peak temperatures with and without thermal hold, respectively. Therefore, the maximum nucleation rate is expected to occur for the lowest T_{p1} obtained after thermal holding at a given nucleation temperature, which, for sample 1.2, was determined as ~646°C.

3.7. Nanocrystalline glass ceramic

3.7.1. Crystalline phase identification and crystal size determination

A transparent glass ceramic with the composition $40GeO_2$–$10SiO_2$–$25Nb_2O_5$–$25K_2O$ was prepared (Fig. 12) starting from the parent glass sample, followed by a ceramization step at the maximum nucleation rate temperature (646 °C) for 2 h. The crystalline phase obtained was identified by XRD (Fig. 13) as $K_{3.8}Nb_5Ge_3O_{20.4}$.

Crystal size (t) was determined, using the Scherrer formula [24]:

$$t = \frac{0.9\lambda}{B\cos\theta_B} \tag{6}$$

where λ is the wavelength of the Cu Kα radiation, B is the width at half height of the diffraction peak and θ_B is the angle at which its maximum intensity occurs. From Eq. (6), a value of ~5 nm was determined, but this approach did not account for the strain broadening and, in fact, TEM results (Fig. 14) led to higher values of the order of ~20–25 nm.

Although nanocrystallization could be obtained in a transparent glass ceramic, the crystalline phases produced are neither the $KNbSi_2O_7$ nor the $KNbO_3$ non-linear phases. In fact, the former phase was only obtained for long heat treatments (more than 4 h) at high temperatures (~1100 °C) in agreement with Aronne et al. [9], while the latter has only been obtained for compositions with high K_2O content (> 40 mol%) [4].

3.7.2. Crystallized volume fraction determination

The crystallized volume fraction (f) of the glass ceramic obtained was determined by density measurements, using the formula [3]:

$$f = \frac{\rho_{sample} - \rho_{glass}}{\rho_{crystal} - \rho_{glass}} \tag{7}$$

where ρ_{sample} is the glass ceramic density, ρ_{glass} is the density of the glass sample untreated and $\rho_{crystal}$ is the density of a sample heat treated at 850 °C for 5 h. Due to stoichiometric differences between crystalline phase and the glass matrix it was considered that a maximum amount of 74% could be crystallized. Therefore, a crystallized volume fraction of ~57% was determined for the $40GeO_2 \cdot 10SiO_2 \cdot 25Nb_2O_5 \cdot 25K_2O$ composition, heat treated at 646° for 2 h (Table 5). This result is in good agreement with the data reported by Narita et al. [3] for the $50GeO_2 \cdot 25Nb_2O_5 \cdot 25K_2O$ composition.

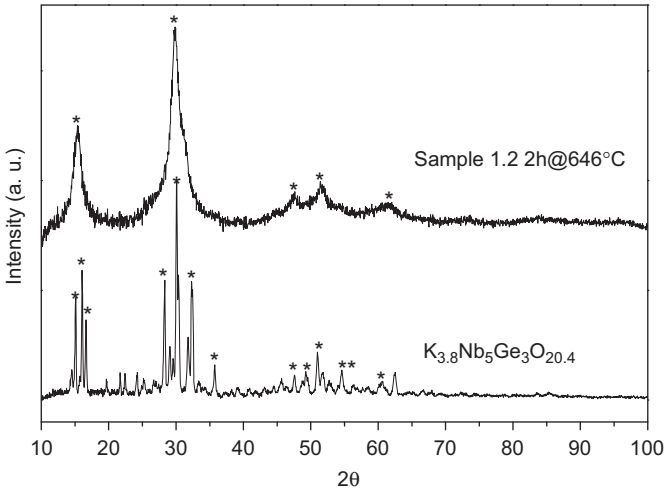

Fig. 13. XRD pattern of the glass ceramic produced.

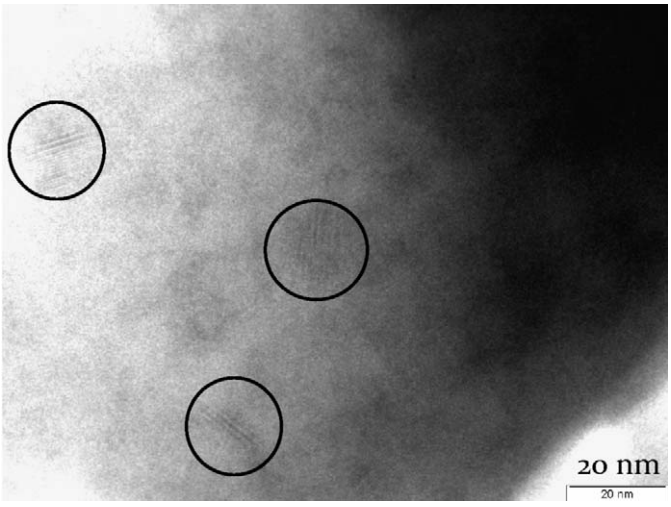

Fig. 14. TEM image of the glass ceramic produced (circles indicate nanocrystals).

Considering a glass ceramic with an average crystal size of 25 nm (TEM results) and 0.57 of crystal volume fraction (density data), one can estimate the nucleation rate, I, assuming a zero induction time for homogeneous nucleation, using the following expression [25]:

$$I \sim N_V(t)/t_{HT}, \tag{8}$$

where t_{HT} is the heat-treatment time and $N_V(t)$ is the number of crystals per unit volume after a time t. $N_V(t)$ can be estimated dividing the crystal volume fraction by the volume of a single crystal, which can be approximated to a sphere. Therefore, fixing r=15 nm, t_{HT}=7200 s and a crystal volume fraction of 0.57, one obtains a nucleation rate of $9.7 \times 10^{18}\,m^{-3}\,s^{-1}$. This is a very high value for an inorganic glass, even higher than the one reported for fresnoite glass [26], which is in agreement with the relatively low glass-forming tendency (as judged by the $T_x - T_g$ parameter, Table 2) and the fact that the present glass exhibit volume crystallization, The high value of the observed nucleation rate could be due to effects of chemical diffusion since the chemical composition of the crystal phase is slightly different from that of the parent glass (see Ge/Nb ratio). If the crystal is enriched in network modifiers it will create a rigid shell around the crystals, which prevents further crystal growth and coarsening. The

Table 5
Density results for the determination of the crystallized volume fraction.

Sample	Density (g/cm^3)	Crystal volume fraction (%)	Correction (74% maximum)
Glass	3.684 (ρ_{glass})	0	0
2 h/646 °C	3.812 (ρ_{sample})	77.6	57
5 h/850 °C	3.849 ($\rho_{crystal}$)	100	74

transformable volume will decrease slower with time, which leads, in principle, to a higher nucleation rate. The initial step could also be related to an incipient phase separation which could induce nucleation by creating a multiplicity of nucleation sites; however, chemical gradients around the crystals have not been studied.

5. Conclusion

Glass samples in the $GeO_2 \cdot SiO_2 \cdot Nb_2O_5 \cdot K_2O$ system were prepared and their characteristic temperatures were determined by DTA. An increase in T_g and $T_x - T_g$ with the replacement of GeO_2 by SiO_2 was observed. The crystalline phases related to the first exothermic peaks were identified by both XRD and Raman spectroscopy, indicating the formation of $K_{3.8}Nb_5Ge_3O_{20.4}$ for the high germania content compositions and $K_3Nb_3Si_2O_{13}$ for the high silica compositions. Even for the stoichiometric composition of the $KNbSi_2O_7$ crystalline phase ($66.7SiO_2 \cdot 16.6Nb_2O_5 \cdot 16.6K_2O$) the first crystalline phase to occur was $K_3Nb_3Si_2O_{13}$.

The $40GeO_2 \cdot 10SiO_2 \cdot 25Nb_2O_5 \cdot 25K_2O$ glass composition presented the better ability to undergo bulk crystallization. An activation energy for crystallization of $\sim$528 kJ/mol and a nucleation rate of $9.7 \times 10^{18}\,m^{-3}\,s^{-1}$ was obtained, for this composition after a 2 h heat-treatment at the maximum nucleation rate temperature. A transparent glass ceramic with a crystal volume fraction of $\sim$57% and nanocrystal sizes of $\sim$20–25 nm was produced.

Acknowledgments

This work was developed under the GRICES/DAAD programme and the project PTDC/CTM/64235/2006 funded by the Portuguese Fundação para a Ciência e a Tecnologia Foundation for Science and Technology (FCT).

References

[1] M.C. Goncalves, L.F. Santos, R.M. Almeida, Comptes Rendus Chimie 5 (2002) 845–854.
[2] N.V. Golubev, V.N. Sigaev, S.Y. Stefanovich, T. Honma, T. Komatsu, Journal of Non-Crystalline Solids 354 (2008) 1909–1914.
[3] K. Narita, Y. Takahashi, Y. Benino, T. Fujiwara, T. Komatsu, T. Hanada, Y. Hirotsu, Journal of the American Ceramic Society 87 (2004) 113–118.
[4] H. Tanaka, M. Yamamoto, Y. Takahashi, Y. Benino, T. Fujiwara, T. Komatsu, Optical Materials 22 (2003) 71–79.
[5] P. Pernice, A. Aronne, V. Sigaev, M. Kupriyanova, Journal of Non-Crystalline Solids 275 (2000) 216–224.
[6] D.E. Vernacotola, J.E. Shelby, Physics and Chemistry of Glasses (1994) 153–159.
[7] P. Pernice, A. Aronne, V.N. Sigaev, P.D. Sarkisov, V.I. Molev, S.Y. Stefanovich, Journal of the American Ceramic Society 82 (1999) 3447–3452.
[8] V.N. Sigaev, S.Y. Stefanovich, B. Champagnon, I. Gregora, P. Pernice, A. Aronne, R. LeParc, P.D. Sarkisov, C. Dewhurst, Journal of Non-Crystalline Solids 306 (2002) 238–248.
[9] A. Aronne, V.N. Sigaev, P. Pernice, E. Fanelli, L.Z. Usmanova, Journal of Non-Crystalline Solids 337 (2004) 121–129.
[10] Y. Benino, Y. Takahashi, T. Fujiwara, T. Komatsu, Journal of Non-Crystalline Solids 345 & 346 (2004) 422–427.
[11] I. Enomoto, Y. Benino, T. Fujiwara, T. Komatsu, Journal of Solid State Chemistry 179 (2006) 1821–1829.
[12] A. Aronne, V.N. Sigaev, B. Champagnon, E. Fanelli, V. Califano, L.Z. Usmanova, P. Pernice, Journal of Non-Crystalline Solids 351 (2005) 3610–3618.
[13] K. Narita, Y. Takahashi, Y. Benino, T. Fujiwara, T. Komatsu, Optical Materials 25 (2004) 393–400.
[14] V.N. Sigaev, N.V. Golubev, S.Y. Stefanovich, T. Komatsu, Y. Benino, P. Pernice, A. Aronne, E. Fanelli, B. Champagnon, V. Califano, D. Vouagner, T.E. Konstantinova, V.A. Glazunova, Journal of Non-Crystalline Solids 354 (2008) 873–881.
[15] L.F. Santos, L. Wondraczek, J. Deubener, R.M. Almeida, Journal of Non-Crystalline Solids 353 (2007) 1875–1881.
[16] X.J.J. Xu, C.S. Ray, D.E. Day, Journal of the American Ceramic Society 74 (1991) 909–914.
[17] C.S. Ray, D.E. Day, Thermochimica Acta 280 (1996) 163–174.
[18] C.S. Ray, Q. Yang, W. Huang, D.E. Day, Journal of the American Ceramic Society 79 (1996) 3155–3160.
[19] P. Loiseau, D. Caurant, O. Majerus, N. Baffier, C. Fillet, Journal of Materials Science 38 (2003) 853–864.
[20] M. Rezvani, B.E. Yekta, V.K. Marghussian, Journal of the European Ceramic Society 25 (2005) 1525–1530.
[21] G. Laudisio, M. Catauro, Journal of Thermal Analysis and Calorimetry 52 (1998) 967–974.
[22] A. Marotta, Nucleation and crystallization in glasses, advances in ceramics. The American Ceramic Society, 1982.
[23] M.J. Davis, I. Mitra, Journal of the American Ceramic Society 86 (9) (2003) 1540.
[24] B.D. Cullity, Elements of X-ray Diffraction, third ed., Addison-Wesley Publishing Company Inc., 1967.
[25] P.F. James, Nucleation in Glass-forming Systems—A Review in Advances in Ceramics, The American Ceramic Society Inc., 1982.
[26] A.A. Cabral, V.M. Fokin, E.D. Zanotto, C.R. Chinaglia, Journal of Non-Crystalline Solids 330 (2003) 174–186.